Proceedings of the 28th IEEE
EMBS Annual International Conference
New York City, USA, Aug 30-Sept 3, 2006



# A new scheme and reconstruction algorithm for dual source circular CT

Ming Yan[1], Cishen Zhang[1,2,*], and Hongzhu Liang[1]
[1]School of Electrical and Electronic Engineering
[2]School of Chemical and Biomedical Engineering
Nanyang Technological University, Singapore 639798

*Abstract*— **Circular cone beam scanning has been a most popular scheme for computed tomography (CT) imaging, which is simple and can achieve symmetric projection data of the interested object. Many algorithms have been developed for circular cone beam CT. Many of these are FDK type algorithms, which can achieve good reconstruction quality when cone angle is small but may cause image deformation and density reduction at off plane when the cone angle is large. With the recently introduced dual source circular cone beam CT, we can deal with this problem under a new dual source geometry. In this paper, we propose a novel reconstruction scheme dual source circular cone beam CT by placing X-ray sources on two circular planes perpendicular to the rotating axis. We propose a reconstruction algorithm for this scanning scheme and evaluate the scanning scheme and the reconstruction algorithm with a 3D Shepp Logan phantom and a disk phantom. Simulation results show that the proposed method can provide improved reconstruction image quality for both in plane and off plane of the object.**

*Index Terms*— **Dual source CT, circular cone beam CT, FDK algorithm.**

## I. Introduction

Circular cone beam CT has been popularly employed in clinical applications such as dedicated breast CT and cardiac imaging because of its mechanical simplicity. Circular cone beam CT can not reconstruct exact 3D image because circular orbit does not satisfy the sufficient condition of an exact 3D reconstruction (Tuy's condition)[7]. The FDK algorithm is developed to reconstruct 3D images for circular cone beam reconstruction. It approximates 2D projection data by multiply 3D projection data with cosine value of the cone angle and reconstruct images with the approximation projection data. The FDK algorithm is efficient and can provide good reconstruction image for small cone angle. The FDK algorithm and its derivations are widely used for circular cone beam image reconstruction. However, the FDK algorithm can achieve stable image quality for large cone angle. In recent years, many studies have been made to improve reconstruction image quality for circular cone beam CT. In[2] and [5], information lost by FDK reconstruction algorithm is estimated by interpolation methods and used to improve reconstruction image quality. In [8], iterative method and adaptive filter technology are used to improve FDK algorithm reconstruction image quality.

In recent days, dual source cone beam CT are applied into clinical applications [4]. Current dual source circular cone beam CT place two X-ray source on the same transversal plane and can achieve a whole projection data set in a shorter projection interval than single source CT. Dual source circular cone beam CT can achieve better temporal resolution than single source CT. However such geometry place dual sources on the same plane and can not improve reconstruction image quality for large cone angle. In this paper, we proposed a novel geometry for dual source cone beam CT and develop a reconstruction algorithm for this geometry. In this geometry, we place the two X-ray source on two different planes which are perpendicular to the rotating axis, the distance between two planes is determined by clinical requirements. The cone angle can be reduced in this geometry and the proposed method can achieve stable image quality for volume between two source planes.

We have performed computer simulation studies to evaluate the proposed method. The results show that this method can provide stable reconstruction image quality for the whole volume.

## II. Dual source scanning scheme and reconstruction

### A. Geometry of dual source circular CT

The dual source circular CT scanning set up consists of two X-ray sources with the corresponding detector surfaces. In the existing dual source cone beam CT scanning schemes, the dual X-ray sources rotate on the same transversal plane. In this paper, we present a new scanning scheme for the dual source cone beam circular CT.

As shown in Fig. 1, the dual source scanning geometry is setup in a cartesian coordinate system $x-y-z$. The two X-ray sources A and B rotate on circular trajectories on different planes which are perpendicular to the $z$-axis. Let the projection angle of the X-ray source A is $\beta$, its rotating radius be $R_f$ and the z position of the source plane be $z_A$. It follows that the trajectory of the X-ray source A is

$$C_{sA}(\beta) = \begin{pmatrix} x_{sA} \\ y_{sA} \\ z_{sA} \end{pmatrix} = \begin{pmatrix} R_f \cos\beta \\ R_f \sin\beta \\ z_A \end{pmatrix}. \qquad (1)$$

The detector array surface $S_A$ is an arched rectangular surface consisting of $M$ detector rows. The distance between the detector array and $z$ axis is $R_d$ and the thickness of each detector row is $S$. The position of each cell $C_A(\beta, \theta_A, u_A)$ on the detector surface $S_A$ can be represented by $\beta$, projection fan angle $\theta_A$, as shown in Fig. 1, and the height of the

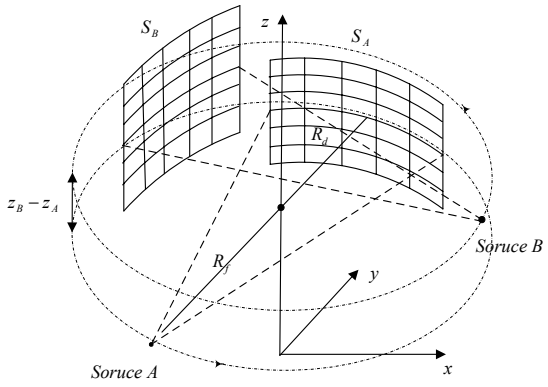


Fig. 1. Illustration the geometry of dual source CT

detector array surface $u_A \in [0,(M-1)S]$, as in the following.

$$\begin{pmatrix} x_{Ac} \\ y_{Ac} \\ z_{Ac} \end{pmatrix} = \begin{pmatrix} R_f\cos\beta - (R_f+R_d)\cos(\beta-\theta_A) \\ -R_f\sin\beta + (R_f+R_d)\sin(\beta-\theta_A) \\ u_A + Z_A - (M-1)S/2 \end{pmatrix}. \quad (2)$$

The framework of the X-ray source B and its detector array surface $S_B$ is identical to that of the X-ray source A and its detector array surface. The X-ray source B is placed on the plane $z = z_B > z_A$, whose projection angle is $\beta + \frac{\pi}{2}$ with an angular difference $\frac{\pi}{2}$ from the X-ray source A. The trajectory of the X-ray source B is

$$C_{sB}(\beta) = \begin{pmatrix} x_{sB} \\ y_{sB} \\ z_{sB} \end{pmatrix} = \begin{pmatrix} -R_f\sin\beta \\ R_f\cos\beta \\ z_B \end{pmatrix}. \quad (3)$$

Correspondingly, each cell $C_B(\beta,\theta_B,u_B)$ on the detector array surface $S_B$ can be represented by $\beta$, projection fan angle $\theta_B$ and the height of the detector array surface $u_B \in [0,(M-1)S]$, as

$$\begin{pmatrix} x_{Bc} \\ y_{Bc} \\ z_{Bc} \end{pmatrix} = \begin{pmatrix} (R_f+R_d)\sin(\beta-\theta_B) - R_f\sin\beta \\ -R_f\cos\beta + (R_f+R_d)\cos(\beta-\theta_B) \\ z_B + u_B - (M-1)S/2 \end{pmatrix} \quad (4)$$

### B. Cone angle of the proposed dual source geometry

With the above introduced dual source scanning geometry, we can derive the cone angle for each point in the object volume. For each point $(x,y,z)^T$ in the volume, the cone angles with respect to X-ray sources A at $(x_{sA},y_{sA},z_A)^T$ and B at $(x_{sB},y_{sB},z_B)^T$, respectively, are

$$\gamma_A = \arctan\left|\frac{z-z_A}{\sqrt{(x-x_{sA})^2+(y-y_{sA})^2}}\right| \quad (5)$$

$$\gamma_B = \arctan\left|\frac{z-z_B}{\sqrt{(x-x_{sB})^2+(y-y_{sB})^2}}\right| \quad (6)$$

We define a angle $\gamma_{min}$ as the minimum value of $\gamma_A$ and $\gamma_B$ as

$$\gamma_{min} = \min\{\gamma_A,\gamma_B\}.$$

For reconstruction of the point $(x,y,z)^T$, the projection data set obtained from the X-ray source with the projection cone angle $\gamma_{min}$ is adopted.

In the existing dual source scanning schemes, the two X-ray sources are placed at the same $z$-position. Without loss of generality, we assume that their are at the plane with $z = (z_A+z_B)/2$, so their positions are $(x_{sA},y_{sA},(z_A+z_B)/2)^T$ and $(x_{sB},y_{sB},(z_A+z_B)/2)^T$, respectively. Correspondingly, we can find cone angles of each point $(x,y,z)^T$ of the object with respect to the sources A and B, denoted as $\gamma_{SA}$ and $\gamma_{SB}$, respectively. And introduce

$$\gamma_{Smin} = \min\{\gamma_{SA},\gamma_{SB}\}.$$

This angle $\gamma_{Smin}$ determines the data set of the corresponding X-ray source to be adopted for reconstruction of the object point.

To compare projection cone angles of our propose scheme with the existing scheme, we further introduce $\gamma_{max}$ to be the maximum acceptable projection cone angle for image reconstruction. Let $r$ be the radius of the support cylinder of the object. Following form the above described cone angle dependent projection data set selection scheme, it can be verified that the volume within

$$z \in \left(\frac{z_A+z_B}{2} - 2(R_f-r)\tan\gamma_{max}, \frac{z_A+z_B}{2} + 2(R_f-r)\tan\gamma_{max}\right)$$

can reconstructed with the acceptable projection cone angle by our proposed scanning scheme. In contrast, the accepted volume of the existing scanning scheme is

$$z \in \left(\frac{z_A+z_B}{2} - (R_f-r)\tan\gamma_{max}, \frac{z_A+z_B}{2} + (R_f-r)\tan\gamma_{max}\right).$$

This clearly shows that our proposed scheme can effectively reduce the projection cone angle for reconstruction.

## III. Dual source CT image reconstruction

### A. Rebinning projection data set

In our reconstruction algorithm, we select source trajectory segment for each point on which we can reconstruct the point with reduced cone angle. For cone beam geometry, because Parker's weighting is applied to projection data before filter operation to deal with data redundancy for shot scan, the filtered data for one source trajectory segment can not be used by another. On the other hand, for parallel geometry, a point can be reconstruct without Parker's weighting. We reform a cone parallel data set from original projection set to reduce the computation quantity on refiltering.

The projection ray radiates on the cell $C_A(\beta,\theta,u)$ of detector A. This projection ray can be converted to cone parallel geometry and is parameterized projection angle $\alpha$, the distance from the projection ray to rotation axis $t$ and height on the detector $u$. As shown in Fig. 2, the in-plane correspondence between ray's cone beam coordinates and cone parallel coordinates is:

$$\alpha = \frac{\pi}{2} + \beta + \theta \quad and \quad t = -Rf\sin\theta \quad (7)$$

Let the projection datum collected from the real detector cell on detector $S_A$ at the projection angle $\beta$ be denoted by $D_A(\beta,\theta,u)$ and the corresponding projection datum on the virtual detector cell for the cone-parallel geometry $(\alpha,t,u)^T$

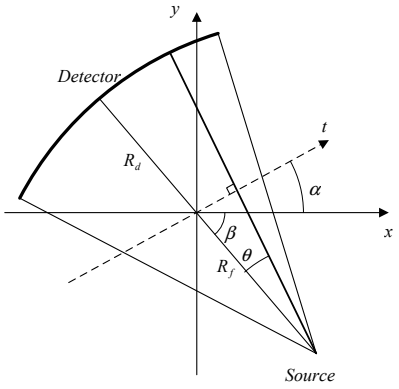


Fig. 2. Illustration the in-plane conversion from native cone beam geometry to cone parallel geometry

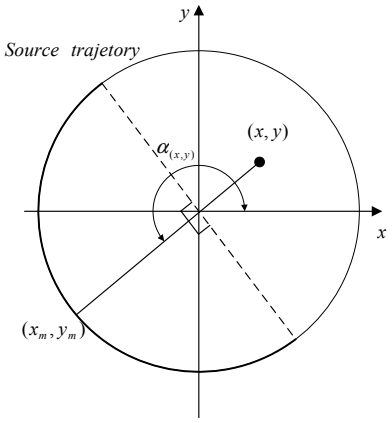


Fig. 3. Illustration the different cone angle for different projection interval.

the same projection ray be denoted by $D_{vA}(\alpha,t,u)$. Since $D_A(\beta,\theta,u)$ and $D_{vA}(\alpha,t,u)$ are due to the same projection ray, we have

$$D_{vA}(\alpha,t,u) = D_A(\beta,\theta,u). \tag{8}$$

This can be used to obtain the reformed projection data set for the cone-parallel geometry. Because the X-ray source B and detector $S_B$ have same structure and size, we can reform cone beam parallel projection data with the same procedure.

### *B. Reconstruction*

Using the reformed projection data set, we can reconstruct a point $(x,y,z)^T$ of the interest volume with the following FDK reconstruction algorithm for cone parallel geometry

$$f(x,y,z) = \int_{\alpha_{(x,y)}-\frac{\pi}{2}}^{\alpha_{(x,y)}+\frac{\pi}{2}} \frac{u}{\sqrt{(R_f+R_d)^2+u}} \tilde{D}_{wv}(\alpha,t,u)d\alpha, \tag{9}$$

where

$$\begin{aligned} \tilde{D}_{wv}(\alpha,t,u) &= \frac{w(\alpha,t,u_A)\tilde{D}_{vA}(\alpha,t,u_A)+w(\alpha,t,u_B)\tilde{D}_{vB}(\alpha,t,u_B)}{w(\alpha,t,u_A)+w(\alpha,t,u_B)}, \\ \tilde{D}_{vA}(\alpha,t,u) &= D_{vA}(\alpha,t,u)\otimes g(t), \\ \tilde{D}_{vB}(\alpha,t,u) &= D_{vB}(\alpha,t,u)\otimes g(t) \end{aligned} \tag{10}$$

$\otimes$ denotes the convolution operation and the angle $\alpha = \alpha(x,y)$ is the centre projection angle for reconstructing the point $(x,y,z)^T$.

For circular cone beam CT, we reconstruct image with reformed cone parallel data set and the range of projection angle is $\pi$. We can reduce the cone angle by selecting the centre projection angle $\alpha_{(x,y)}$ for each point $(x,y,z)^T$. The cone angle for X-ray source source A $\gamma_A$ defined in Eq. 5 is minimized when the distance between $(x_{Ap},y_{Ap})$ and $(x,y)$ is maximized. As shown in Fig. 3, the distance is maximized at $(x_m,y_m)$. With Eq. 6, the cone angle for X-ray source B is minimized at the same projection angle. We define the projection angle for $(x_m,y_m)$ as the centre projection angle and the projection angle range to reconstruct $(x,y,z)^T$ is $[\alpha_{(x,y)}-\pi/2, \alpha_{(x,y)}+\pi/2]$ mark with dark curve in Fig. 3. The centre projection angle is:

$$\alpha_{(x,y)} = \begin{cases} \pi + \arcsin\frac{y}{\sqrt{x^2+y^2}} & x >= 0 \\ 2\pi - \arcsin\frac{y}{\sqrt{x^2+y^2}} & x < 0 \end{cases} \tag{11}$$

The $w(\alpha,t,u)$ is the weighting function.

$$w(\alpha,t,u) = \begin{cases} 1 & |u-\frac{(M-1)S}{2}| < 0.4(M-1)S \\ 1.0-\frac{u}{(M-1)S} & 0.4(M-1)S \le |u-\frac{(M-1)S}{2}| < (M-1)S \\ 0 & else \end{cases} \tag{12}$$

In this equation, $u_A$ is the hight of projection ray passing through $(x,y,z)^T$ on detector A and $u_B$ is the hight of projection ray passing through $(x,y,z)^T$ on detector B.

## IV. Simulation and Results

We use 3D Shepp Logan phantom and disk phantom to evaluate the performance of the the proposed dual source circular CT geometry and its reconstruction algorithm.

The size of the Shepp Logan phantom is 200mm×200mm×200mm. The radius of the X-ray source $R_f$ is 400mm and $R_d$ is 200mm. The slice number $M = 256$ and slice thickness $S$ is 1mm. The maximum cone angle is 12.04°. The number of projections is 300 per cycle and the number of projections in a projection fan is 400. For the dual CT, the z position for X-ray source A is -50 mm and the z position of X-ray source B is 50 mm. The z position of single source CT is 0 mm.

As shown in Fig. 4, we show the original image of $x = 0$ mm of 3D Shepp Logan phantom in Fig. 4(a). The Fig. 4(b) is reconstructed by dual source CT with proposed reconstruction algorithm and the Fig. 4(c) is reconstructed by single source CT with FDK algorithm. We plot profiles for these images at $y = 0$ mm in Fig. 4(d). In the Fig. 4(d), the original profile is denoted by solid line, the profile achieved with dual source CT is denoted by dashed line and the profile achieve with single source CT is denoted by dotted line. From the reconstructed images and profiles, the results for the single source with FDK algorithm show obvious density drop for large cone angle. The dual source CT with proposed algorithm provide better reconstruction image than the single source CT.

We use Disk phantom to evaluate the performance of the dual source CT. The size of the Disk phantom is

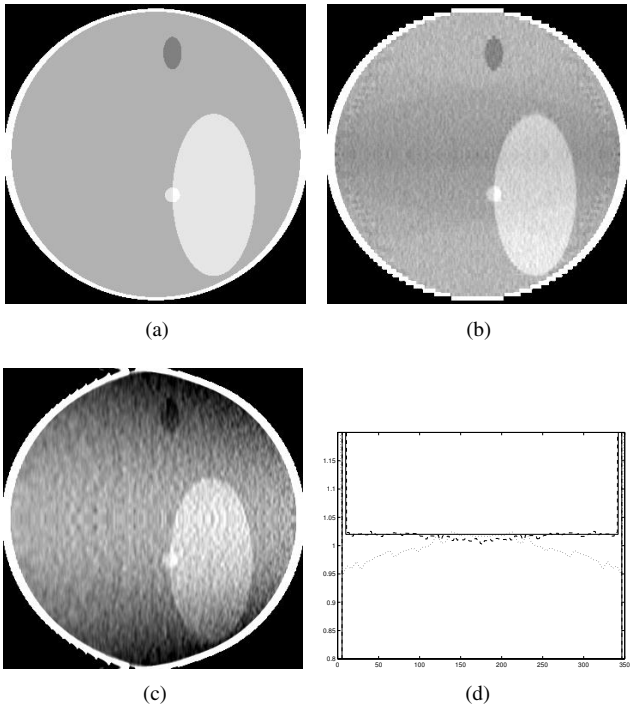

(a) (b) (c) (d)

Fig. 4. Images for $x = 0$ of Shepp Logan phantom with $M = 256$. (0.95-1.05)

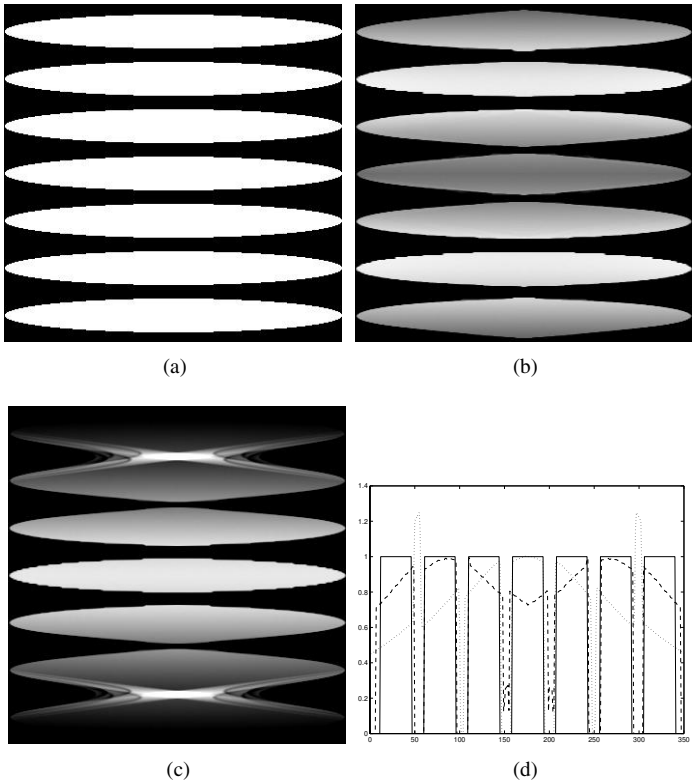

(a) (b) (c) (d)

Fig. 5. Images for $x = 0$ of disk phantom with $M = 256$. (0.5-1.05)

20mm×20mm×20mm. The radius of the X-ray source $R_f$ is 400mm and $R_d$ is 200mm. The slice number $M = 256$ and slice thickness $S$ is 1mm. The maximum cone angle is 12.04°. The number of projections is 300 per cycle and the number of projections in a projection fan is 400. For the dual CT, the z position for X-ray source A is -50 mm and the z position of X-ray source B is 50 mm. The z position of single source CT is 0 mm.

As shown in Fig. 5, we show the original image of $x = 0$ mm of Disk phantom in Fig. 5(a). The Fig. 5(b) is reconstructed by dual source CT with proposed reconstruction algorithm and the Fig. 5(c) is reconstructed by single source CT with FDK algorithm. We plot profiles for these images at $y = 0$ mm in Fig. 5(d). In the Fig. 5(d), the original profile is denoted by solid line, the profile achieved with dual source CT is denoted by dashed line and the profile achieve with single source CT is denoted by dotted line. From the reconstructed images and profiles, the results for the single source with FDK algorithm show obvious density drop for large cone angle. The dual source CT with proposed algorithm provide better reconstruction image than the single source CT. Because the Disk phantom is sensitive to cone angle, the profile shows obvious density drop with the increasing cone angle.

## V. Conclusion

In this paper we presents a novel dual source CT geometry and develop a FDK type reconstruction algorithm. Because the dual source CT geometry can effectively reduce cone angle for the interest volume, it can reduce reconstruction image density drop and deformation caused by large cone angle. The simulation results demonstrate the proposed dual source CT geometry improve can improve reconstruction image quality considerably.

Although the cone angle is reduced by dual source CT, there still exists some density drop and deformation as shown in Fig. 5. In the future we will develop an algorithm on this geometry to reduce these cone angle artifacts.

## References


[1] X. Pan, D. Xia, Y. Zou, L. Yu, "An unified analysis of FBP-based algorithms in Helical cone-beam and circular cone and fan beam scans ", *Phys. Mid. Biol.*, Vol. 49, 2004, 2717-2731.

[2] H. Hu, "an improved cine-beam reconstruction algorithm for the circular orbit ", *Scanning*, vol. 18, 1996, pp 572-581.

[3] L. A. Feldkamp, L. C. Davis, and J. W. Kress, "Practical cone-beam algorithm ", *J. Opt. Soc. Am.*, A1, 1984, pp 612-619.

[4] S. Achenbach, D. Ropers, A. Kuettner, T. Flohr, B. Ohnesorge, H. Bruder, H. Theessen, M. Karakaya, W. G. Daniel, W. Bautz, W. A. Kalender, K. Anders, "Contrast-enhanced coronary artery visualization by dual-source computed tomography¦Initial experience ", *European Journal of Radiology*, Vol 57, 2006, pp 331-335.

[5] H. Yang, M. Li, K. Koizumi, H. Kudo, "A FBP-type cone-beam reconstruction algorithm with radon space interpolation ability for axially trunacated data from a circular orbit ", *Full 3D imaging 2005*, 2005, pp 401-404.

[6] M. Grass, T, Kohler, R. Proksa, "3D cone-beam CT reconstruction for circular trajectories ", *Phys. Mid. Biol.*, Vol 45, 2000, pp 329-347.

[7] H. K. Tuy, "an inversion formula for cone-beam reconstruction ", *SIAM J. Appl. Math*, Vol. 43, 1983, pp 546-552.

[8] Kai Zeng, Zhiqiang Chen, Li Zhang, Ge Wang, "An error-reduction-based algorithm for cone-beam computed tomography ", *Med. Phys.*, Vol. 31, 2004, pp 3206-3212.